Electron cyclotron resonance harmonics and wall material effects in a microwave discharge

Ane Aanesland[a] and Åshild Fredriksen
Physics Department, University of Tromsø, N-9037 Tromsø, Norway

(Received 16 April 2003; accepted 11 July 2003)

In this article we investigate a 2.45 GHz microwave discharge operated at the electron cyclotron resonance (ECR) and the second harmonic, by applying a divergent magnetic field where the maximum is changed from 1400 to 500 G. The magnetic field is continuously decreased so that the ECR zone is moved axially along the chamber from about 15 cm away to very close to the microwave window. When the field is reduced to below 875 G the ECR disappears and only the second harmonic is present in the source. We observe that the second harmonic is not efficient enough for breakdown at microwave power of less than 500 W and gas pressure of 0.48 Pa, and it is shown that an overdense plasma can not be generated by use of the second harmonic (independent of gas type). It is also shown that the wall material close to the ECR zone is extremely important, probably due to an effect similar to that of the antenna material in capacitively and inductively coupled plasma sources. The possibility of measuring the thickness and location of the effective ionizing resonance zone is discussed. A calculation of the plasma density as a function of the magnetic field is performed, which takes into account the conservation of magnetic flux and the secondary emission from the wall, and excellent agreement with the measured results is obtained.
© *2003 American Institute of Physics.* [DOI: 10.1063/1.1611613]

I. INTRODUCTION

Microwave discharges were developed in the 1960s and are widely used in the semiconductor industry today. In the early days these sources were usually operated under electron cyclotron resonance (ECR) conditions where the electrons are continuously accelerated by the microwave electric field.[1] Extensive research and development have been done to improve and optimize the ECR sources for a wide range of applications. It has been shown that the most important plasma parameters, like ion energies, plasma densities, electron temperatures, homogeneity etc., depend substantially on the microwave introduction method[2,3] and magnetic field configuration.[4–8]

The magnetic field configurations described and studied in the literature span over a variety of radially and axially uniform magnetic fields, divergent, mirror, and cusp fields. The preferred field configuration depends on the purpose of the plasma source, but very often the microwaves are launched parallel to the magnetic field lines so that the ECR condition, $\omega=\omega_{ce}=eB/m$, is obtained once or several times in the source, for 2.45 GHz that is, $B_{ce}=875$ G. There have been reports on microwave discharges obtained in uniform and mirror magnetic fields, where the field intensity is slightly higher or lower than B_{ce}, and where breakdown and microwave absorption appear in the vicinity of the ECR at $\omega_{ce}/\omega=0.8-1.4$.[9,5] Second harmonics of the ECR coexisting with the fundamental resonance, giving rise to an additional maximum in the ion beam current where the harmonic resonance occur, have been reported using cusp or mirror field configurations.[8] Increased local ion beams due to harmonic resonances have not been observed in divergent magnetic fields.

Although much has been written about the dependency of the magnetic field configuration in ECR sources, little attention has been paid to investigations where harmonics of the ECR is exclusively present in the source, and operation at low magnetic fields is still poorly understood. In this article we consider the effect from a variable divergent magnetic field where the position of the ECR can be moved along the chamber axis as a function of the distance from the microwave introduction window. We investigate the plasma parameters as the ECR position changes from about 15 cm to very close to the introduction window, to well below the point where the ECR disappears, $B_{max}<875$ G, and only the second harmonic, at $B=437$ G, is present in the source. As the ECR zone moves axially along the source chamber, the wall material changes from stainless steel to copper due to a copper gasket. In this work we also demonstrate that the wall material in ECR sources might be of importance for plasma optimization in a similar manner as for the antenna materials in capacitively and inductively coupled rf plasmas.[10,11]

II. EXPERIMENT

With the exception of the microwave insertion, the ECR plasma source has been described in detail elsewhere,[12] and is shown in Fig. 1. Briefly, rectangular TE_{10} microwave modes, at 2.45 GHz, are fed into the vacuum chamber via a 6.8 mm thick rectangular quartz window connected to a cylindrical port of 10 cm diameter. The microwaves enter the

[a]Author to whom correspondence should be addressed; electronic mail: ane@phys.uit.no

Downloaded 21 Nov 2003 to 198.35.7.27. Redistribution subject to AIP license or copyright, see http://ojps.aip.org/rsio/rsicr.jsp

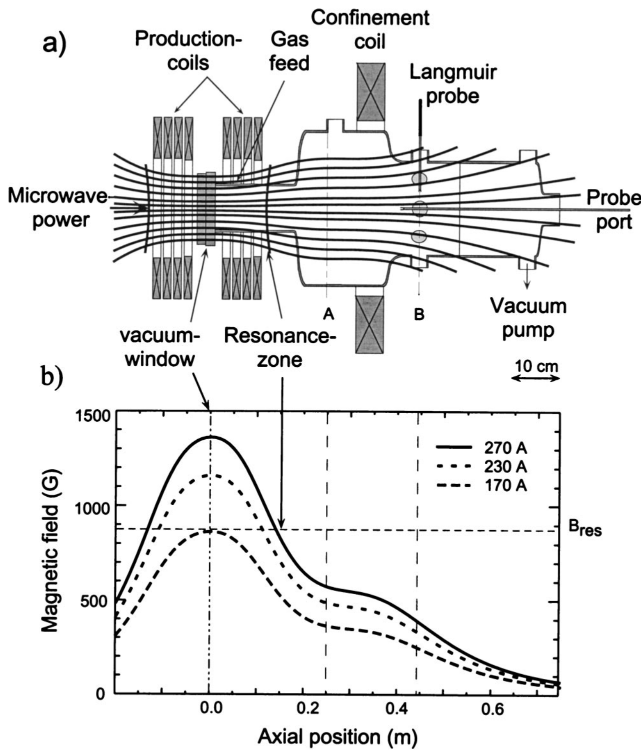

FIG. 1. A schematic drawing of the ECR device with the magnetic field configuration.

narrow part of the vacuum chamber, 10 cm in diameter and 15 cm long. The diffusion chamber is 30 cm in diameter and 70 cm long.

Two sets of four coils supply a divergent magnetic field configuration, while one extra coil provides improved plasma confinement. The nine coils are connected in series having the same current flow, which is changed from 280 to 100 A, corresponding to a maximum magnetic field from 1400 to 500 G. The maximum field is placed at the microwave window to protect the window from damage due to sputtering. The gas flow is monitored by two MKS mass-flow controllers. The operation pressure is measured by a Baratron and the base pressure by an ion gauge. The total gas pressure is 0.48 Pa where two gas mixtures are used: (i) 90% Ar, 10% N_2 and (ii) 90% N_2, 10% Ar, which will be referred to as the Ar and N_2 dominant case, respectively. The microwave power is constant at 500 W where 10–15 W is reflected.

A cylindrical Langmuir probe (LP) 25 cm from the microwave window, on the axis of symmetry, is used to obtain the plasma density (n_i), plasma potential (V_p), floating potential (V_f), and electron temperature (T_e). A nonmagnetized theory for analyzing the LP characteristics is used. However, to compensate for the magnetic field the plasma density is found by use of the ion saturation current with an effective probe area corresponding to the projection of the probe surface in the direction of the magnetic field.[13] The LP analysis is described in more detail in previous works.[12,14]

III. RESULTS AND DISCUSSION

The plasma density, plasma potential, floating potential and electron temperature are shown in Fig. 2 as a function of the current in the magnetic field coils. The Ar and N_2 dominant cases are shown as diamonds and triangles, respectively. Each experimental set is carried out starting at 280 A, reducing the current to 100 A, avoiding any hysteresis effects. As

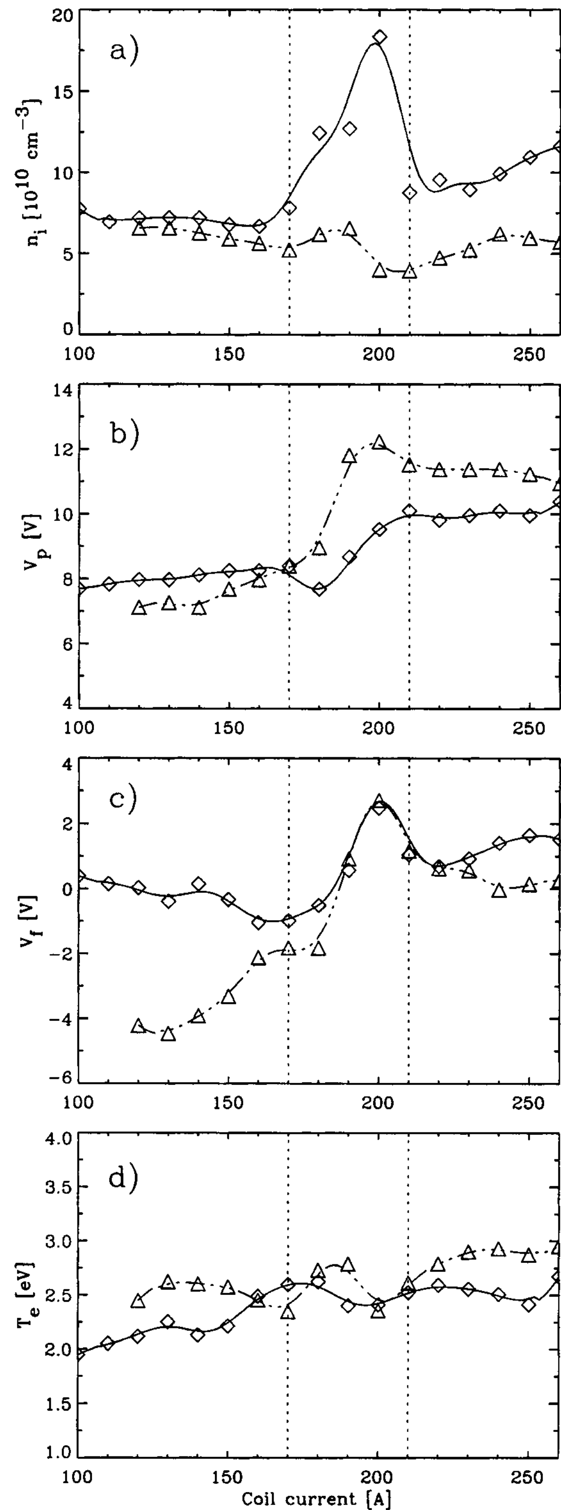

FIG. 2. (a) Plasma density n_i, (b) plasma potential V_p, (c) floating potential V_f, and (d) electron temperature T_e as a function of the coil current, with constant microwave power of 500 W and constant pressure of 0.48 Pa. Diamonds are results obtained with 90% Ar and 10% N_2, while triangles are obtained with 90% N_2 and 10% Ar.

Downloaded 21 Nov 2003 to 198.35.7.27. Redistribution subject to AIP license or copyright, see http://ojps.aip.org/rsio/rsicr.jsp

indicated by the dotted lines in Fig. 2 the result can be divided into three regimes: (1) below 170 A, (2) between 170 and 210 A, and (3) above 210 A.

The plasma density, Fig. 2(a), is higher in the Ar than in the N_2 dominant case. Below 170 A, n_i is constant or slightly decreasing with increasing coil current. Between 170 and 210 A, n_i increases rapidly (~50%) with the coil current in the Ar dominant case, while n_i increases by 15% and then decreases by 40% in the N_2 dominant case. Above 210 A, n_i increases linearly by ~30% with the coil current in both cases. The plasma potential, Fig. 2(b), slightly increases with increasing coil current below 170 A. Between 170 and 210 A, V_p increases rapidly from about 8 to 10 V and 8–12 V in the Ar and N_2 dominant case, respectively, and V_p is constant above 210 A. Below 170 A, V_p is highest for the Ar dominant plasma, while above 170 A it is higher in the N_2 case. The plasma potential [Fig. 2(b)], floating potential, (c), and electron temperature (d) are related within 20% as $V_p - V_f \sim 5kT_e$.

Note that below 170 A breakdown has not been achieved, and for pressure below ~0.1 Pa the plasma easily switches off when reducing the coil current below this value. Below 100 A the plasma is severely difficult to sustain, and the coil current and the tuning have to be changed carefully. However, the plasma has been sustained at currents as low as 10 A, i.e., $B_{max} < 50$ G.

A. The second harmonic resonance

The resonance position in the source is obtained by calculating the magnetic field strength from Amperes law. The resonances are obtained at magnetic fields given by $B_k = m\omega/ek$, where the integer $k = 1,2,3,...$ indicates the fundamental resonance, the second, third harmonics and so on. Generally, 95% of the microwave power is absorbed at the resonance surface located closest to the microwave introduction.[5] However, by generating a mirror trap magnetic field it has been reported that the ECR surfaces might change to multiring structures and an increase in the ion beam can be observed where the lower harmonics are located.[15] These "local" ion beam currents have not been observed in decreasing magnetic fields where the ECR exist in the source. Therefore only the first resonance that appears after the microwave introduction window is calculated, and the position of the resonance zone as a function of the coil current is shown in Fig. 3, where the zero position is at the microwave window. 172 A is the minimum current for which the ECR is obtained in the source, and the ECR zone moves from about 4 to 15 cm from the window when the current is increased from 180 to 280 A. The second harmonic, at 437 G, is present at coil currents between 90 and 172 A, and the third harmonic at 218 G, between 60 and 90 A. Below 60 A several lower harmonics are closely spaced and obtained in the narrow part of the chamber, simultaneously. Experimentally we observe that the plasma switches off either at 170 A or when reaching the third harmonics at 100 A, not inbetween. Although reports on microwave absorption in the vicinity of ECR, where $\omega_{ce}/\omega = 0.8$ throughout the entire plasma have been published,[9] our plasma is maintained by the second

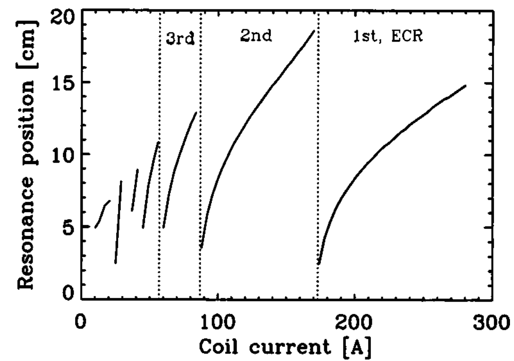

FIG. 3. The calculated resonance position as a function of coil current, where zero position is at the microwave window. Only the resonance zone closest to the window is shown, and the fundamental ECR, the second and third harmonics are indicated between the dotted lines.

harmonics below 170 A, due to the above experimental observations.

The second harmonic is not efficient enough to break down the argon nor the nitrogen gas, but the microwaves can be absorbed if the plasma already exists. This can be explained by considering the basic principle of the ECR heating which is described in detail elsewhere.[5,1] Briefly, the linearly polarized microwave field launched into the source chamber parallel to the magnetic field can be represented as a superposition of right- and left-hand circularly polarized (RHP and LHP) waves, respectively. The LHP wave is not directly absorbed at ECR,[5] and the influence of this wave will not be discussed here. At the ECR position, where the frequency of the gyrating electrons and the RHP wave is equal, $\omega_{ce}/\omega = 1$, there is a continuous energy gain from the wave to the electrons, and the microwaves are effectively absorbed. No collisions are needed to ensure energy transfer at this resonance, so ECR plasmas can be obtained at very low pressure.[1] However, at the second harmonics, $\omega_{ce}/\omega = 0.5$, the electrons are both accelerated and decelerated, so for the wave to continuously add energy to the plasma, collisions are necessary. Since the collision frequency increases with pressure, the harmonic resonance can absorb energy from the wave above a threshold pressure, but are not efficient enough for breakdown, at least for microwave power less than 500 W.

In nonmagnetized plasmas the electromagnetic waves cannot penetrate the plasma if the wave frequency ω is less than the plasma frequency, $\omega_{pe} = \sqrt{e^2 n_e/\epsilon_0 m_e}$. The critical density n_c is therefore given as

$$n_c = \frac{m_e \epsilon_0 \omega^2}{e^2} = 7.4 \times 10^{10} \text{ cm}^{-3} \quad \text{at } 2.45 \text{ GHz}, \qquad (1)$$

and plasmas with densities higher than this value are called overdense plasmas. There is no density limitation for the RHP waves launched and propagating along magnetic field lines.[5] However, it has been shown experimentally that at low magnetic fields where $\omega_{ce}/\omega < 1$ the RHP wave is reflected on the boundary of the overdense plasma, as for unmagnetized plasmas.[9] At coil currents below 170 A, i.e., at low magnetic fields, the plasma densities in the Ar and N_2 dominant cases are almost equal, and approaching n_c, which

Downloaded 21 Nov 2003 to 198.35.7.27. Redistribution subject to AIP license or copyright, see http://ojps.aip.org/rsio/rsicr.jsp

can be explained as follows. As long as $n_i<n_c$ the RHP wave can propagate and become absorbed at the resonance zone. As soon as the plasma density reach the critical density the waves can not easily propagate, due to the low magnetic field, and most of the energy will be reflected. Hence, in the case where the ECR condition is not fulfilled, and the microwave power is high enough, the plasma density will reach a threshold density equal to n_c but will not increase above this value. Instead the excess power will go to heating of chamber walls and waveguides after being reflected back and forth between the plasma boundary and the stub tuners.

At coil currents larger than 170 A the ECR condition is fulfilled and the RHP wave propagates and is effectively absorbed at the resonance. The cross section for the electron impact excitation is generally higher in N_2 than in Ar plasmas; loosely speaking, the creation of an electron–ion pair in a nitrogen plasma has a higher energy cost compared to an argon plasma.[16] Hence, the plasma density typically decreases as N_2 is added to an argon discharge,[16,17] which is in agreement with our results shown in Fig. 2(a).

V_p, V_f, and T_e shows slightly different behavior in the Ar and N_2 case. It is shown elsewhere that a nitrogen plasma with some mixing of argon obtains a slight increase in the electron temperature,[17] and this is in agreement with the result of T_e in Fig. 2. The low V_f in the N_2 case is believed to be related to the electron temperature increase as well as the different quality and characteristics of Ar and N_2 plasmas which is out of the scope of this article.

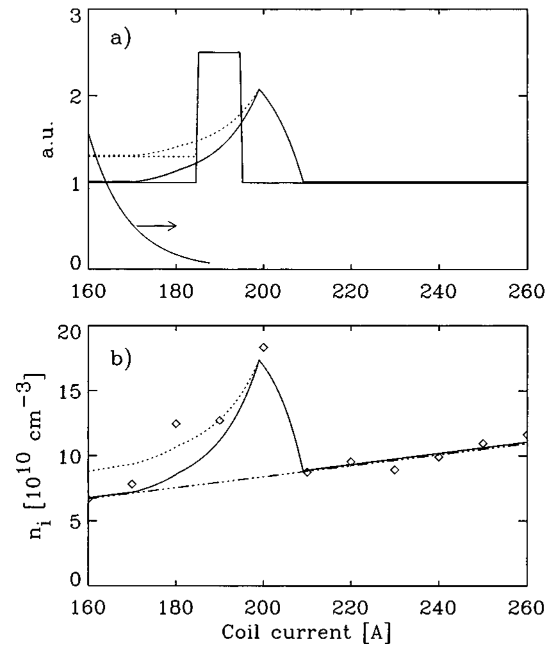

FIG. 4. (a) The secondary emission function $\gamma_{se}(I)$, the effective ionization zone $d_e(I)$, and the convolution of these that gives the plasma production effectivity, $F(I)$. Two cases of $\gamma_{se}(I)$ are shown: (i) solid line $\gamma_{se}(I<185\text{ A})=1$ and (ii) dotted line $\gamma_{se}(I<185\text{ A})=1.3$. (b) The calculated density compared with the measured density in the Ar dominant case, as a function of the coil current above 160 A. Dotted and solid lines correspond to the cases given in (a). The dashed-dotted line corresponds to the density as calculated from Eq. (3) for constant $\gamma_{se}=1$.

B. Wall surface effects

The two regimes above 170 A are both produced at the ECR, so why are two different regimes present in this case?

When increasing the coil current the resonance position moves away from the window closer to the probe, which results in a decreasing loss area along the field line. Assuming conservation of magnetic flux along the chamber axis, the relation between the measured density, n_p, and the density at the resonance surface, n_{ecr}, is

$$\frac{n_{ecr}}{B_{ecr}}=\frac{n_p}{B_p}, \tag{2}$$

where B_{ecr} and B_p are the magnetic fields at the resonance and the probe position, respectively. Since the input power is constant the fraction n_{ecr}/B_{ecr} is constant. The density n_{ecr} can be found from a power balance calculation. However, the calculation is simplified without loss of the physical information, by applying as a reference the data at 210 A, where $n_p=8.5\times10^{10}\text{ cm}^{-3}$ and $B_p=434$ G. The calculated density, n_{cal}, at the probe as a function of the coil current is then

$$n_{cal}(I)=\frac{n_p(210\text{ A})}{B_p(210\text{ A})}B_p(I)=1.96\times10^8 B_p(I). \tag{3}$$

Figure 4(b) shows the measured and calculated plasma density at coil currents above 160 A. The diamonds are the measured densities in the Ar case and the dashed-dotted line is the calculated density from Eq. (3). There is a very good agreement between the measured and calculated density above 210 A (within 10%), which verify that the plasma density changes due to the conservation of magnetic flux.

The plasma density calculated for the N_2 case is shown as the dashed–dotted lines in Fig. 5(b), where $n_{cal}(I)=0.92\times10^8 B_p(I)$ using $n_i=4.0\times10^{10}\text{ cm}^{-3}$ at 200 A as a reference. The calculated and measured plasma density agrees within 30%. However, n_{cal} is somewhat lower than what is measured in the N_2 case, and is probably due to downstream ionization processes, for example collisions between metastable argon atoms and nitrogen, $Ar^*+N\rightarrow Ar+N^++e$, which is not taken into account in the calculation.

Even though the above calculation is in very good agreement with the measured densities above 210 A, both for argon and nitrogen, there is a significant disagreement between the calculation and the measurements at coil currents between 180 and 210 A, particularly in the Ar case.

Focusing first on the argon case, one possible explanation for this dramatic increase in the plasma density at these currents will be given in detail below. The narrow region of the plasma chamber consist of two parts connected with a CF flange, and as a result a copper gasket is directly exposed to the plasma in a narrow area where the plasma production occur at a certain magnetic field. The work function, E_ϕ, and the secondary emission coefficient, γ_{se}, are material dependent and will change along the chamber wall when going from stainless steel to copper. For ion-induced electron emission, γ_{se} depends on E_ϕ and the ionization energy of the impinging atom. For electron-induced electron emission, γ_{se} depends on the electron energy at impingement.[18,11] A change in the secondary emission along the wall might

Downloaded 21 Nov 2003 to 198.35.7.27. Redistribution subject to AIP license or copyright, see http://ojps.aip.org/rsio/rsicr.jsp

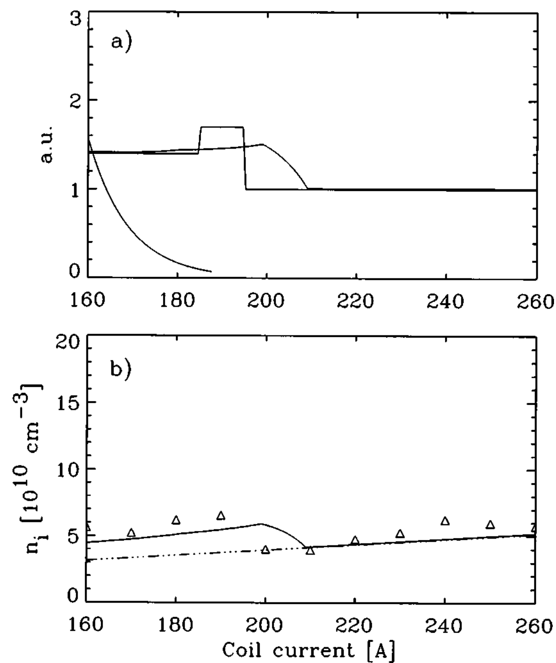

FIG. 5. (a) The secondary emission function $\gamma_{se}(I)$ for the N_2 case, the effective ionization zone $d_e(I)$, and the convolution of these that gives the plasma production affectivity $F(I)$. (b) The calculated density compared with the measured density in the N_2 dominant case, as a function of the coil current above 160 A. The dashed-dotted line corresponds to the density as calculated from Eq. (3), and the solid line corresponds to the calculated density from Eq. (4).

change the ionization efficiency in a manner similar to the multipactor effect in rf plasmas.[10] The only requirement is that the work function of the metal, the ionization energy, or the primary ion or electron energy at impingement results in a $\gamma_{se} \geqslant 1$. In this case we estimate that γ_{se} change relatively from 1 to 2.5 at the interception between stainless steel and copper.[10] Hence, $\gamma_{se}(x)$ is represented as a step function of width $\Delta x = 0.6$ cm, relative height of 2.5, localized at 7 cm where the copper gasket is placed. The resonance position, x, can be replaced by the coil current, I, that obtain 875 G at this position. Hence, the step function can be given as $\gamma_{se}(I)$, where $x = 7$ cm is equivalent to 190 A and $\Delta x = 0.6$ cm equivalent to 10 A as shown in Fig. 4(a). The location, thickness and shape of the resonance zone is set by the magnetic field configuration and might be modified by the Doppler effect for the electrons leading to a broadening of the zone.[1] The wave absorption is determined from the imaginary part of the wave number which decay exponentially along x depending on the magnetic field gradient, frequency, plasma density, and temperature. The interferograms of the wave along the device axis of an ECR etch tool were measured and shows that the wave decays to zero after 1–2 cm when reaching the resonance field.[19] Hence, using the equivalence between the position x and the coil current I as above, we assume that the effective ionization zone decays to zero after 20 A, which correspond to ~1.5 cm. The effective ionization zone, $d_e(I)$, is shown in Fig. 4(a). When the coil current increases the resonance zone moves axially and intercept the copper region at a certain coil current. The plasma production effectivity, $F(I)$, can therefore be estimated as a convolution of $\gamma_{se}(I)$ and $d_e(I)$, which is calculated and shown in Fig. 4(a) as well. The plasma density is now given as

$$n_{\mathrm{cal}}(I) = 1.96 \times 10^8 B_p(I) \cdot F(I), \tag{4}$$

where the density measured at 210 A in the Ar case again is used as a reference. The plasma density calculated from Eq. (4) is plotted as the solid line in Fig. 4(b). The actual value of γ_{se} depends on surface conditions, morphology, impurities, and contaminations[1] and can be difficult to estimate exactly. The above result (solid line) is obtained assuming that γ_{se} is equal for the two assembled parts and only different within a region close to the copper gasket. However, the two parts of the chamber might have a different γ_{se} due to surface contamination. Assuming that $\gamma_{se} = 1.3$ along the part close to the microwave window give the result shown as dotted lines in Fig. 4. As can be seen, the calculated and measured density between 170 and 260 A are in very good agreement. With a "complete" control of the wall surface, i.e., by adjusting the thickness of the copper area etc., the thickness and shape of the resonance zone can be found when moving the ECR zone over the copper area by controlling the magnetic field.

A calculation equivalent to the one above is obtained and shown for the N_2 case in Fig. 5. We can only speculate that the secondary emission coefficient in the N_2 case is different than in the Ar case. If the change in γ_{se} is mostly due to electron-induced electron emission,[10] this coefficient would be lower in the nitrogen case since the electron energy distribution function for N_2 is generally less populated for higher energies compared to an argon plasma. By assuming a $\gamma_{se} = 1.7$ for the copper gasket area we obtain an agreement within 30% between the measured and calculated result as shown in Fig. 5(b).

To further test the proposed mechanism a more accurate control of the magnetic field is needed, and the results can be compared with interferometry measurements.

ACKNOWLEDGMENTS

The authors are grateful for fruitful discussions with C. Charles and V. Guerra, and for the technical assistance by Inge Strømmesen and Kjell Arne Willumstad. This work was supported by the Norwegian Research Council, Grant No. 131953/432.

[1] M. A. Lieberman and A. J. Lichtenberg, *Principles of Plasma Discharges and Materials Processing* (Wiley, New York, 1994).
[2] J. Musil, F. Zacek, and V. N. Budnikov, Czech. J. Phys., Sect. B **23**, 736 (1973).
[3] Y. Torii, M. Shimada, and I. Watanabe, Nucl. Instrum. Methods Phys. Res. B **21**, 178 (1987).
[4] M. Matsuoka and K. Ono, J. Vac. Sci. Technol. A **6**, 25 (1988).
[5] O. A. Popov, J. Vac. Sci. Technol. A **9**, 711 (1991).
[6] M. Murata, S. Uchida, K. Kishimoto, M. Tanaka, A. Komori, and Y. Kawai, Jpn. J. Appl. Phys., Part 1 **31**, 1499 (1992).
[7] N. Hirotsu, T. Yamaguchi, R. Hidaka, and M. Tanaka, Jpn. J. Appl. Phys., Part 1 **33**, 2712 (1994).
[8] G. Neumann and H.-C. Scheer, Rev. Sci. Instrum. **63**, 2403 (1992).
[9] N. Sakudo, Rev. Sci. Instrum. **71**, 1016 (2000).

Downloaded 21 Nov 2003 to 198.35.7.27. Redistribution subject to AIP license or copyright, see http://ojps.aip.org/rsio/rsicr.jsp

[10] R. W. Boswell and D. Vender, Plasma Sources Sci. Technol. **4**, 534 (1995).
[11] R. Krimke and H. M. Urbassek, J. Phys. D **29**, 378 (1996).
[12] A. Aanesland and Å. Fredriksen, J. Vac. Sci. Technol. A **19**, 2446 (2001).
[13] I. H. Hutcinson, *Principles of Plasma Diagnostics* (Cambridge University Press, Cambridge, 1987).
[14] A. Aanesland, C. Charles, R. W. Boswell, and Å. Fredriksen, Plasma Sources Sci. Technol. **12**, 85 (2003).
[15] V. D. Dougar Jabon, A. J. Chacon Velasco, and F. A. Vivas, Rev. Sci. Instrum. **69**, 950 (1998).
[16] K. Tao, D. Mao, and J. Hopwood, J. Appl. Phys. **91**, 4040 (2002).
[17] K. H. Bai, D. S. Lee, and H. Y. Chang, Appl. Phys. Lett. **80**, 3907 (2002).
[18] W. O. Hofer, J. Vac. Sci. Technol. A **5**, 2213 (1987).
[19] J. E. Stevens, Y. C. Huang, R. L. Jarecki, and J. L. Cecchi, J. Vac. Sci. Technol. A **10**, 1270 (1992).

Downloaded 21 Nov 2003 to 198.35.7.27. Redistribution subject to AIP license or copyright, see http://ojps.aip.org/rsio/rsicr.jsp